Ph.D. Dissertation of Science

NSDHL contributes to breast cancer stem-like cell maintenance and tumor-initiating capacity through TGFβ/smad signaling pathway

유방암에서 NSDHL 유전자의 기능 연구

August 2022

Graduate School
Seoul National University College of Medicine
Interdisciplinary Programs in Cancer Biology

So-Hyun Yoon

NSDHL contributes to breast cancer stem-like cell maintenance and tumor-initiating capacity through TGFβ/smad signaling pathway

Advisor Wonshik Han

Submitting a Ph.D. Dissertation

July 2022

Graduate School
Seoul National University College of Medicine
Interdisciplinary Programs in Cancer Biology

So-Hyun Yoon

Confirming the Ph.D. Dissertation written by
So-Hyun Yoon
July 2022

Chair	Young-Joon Surh	(Seal)
Vice Chair	Wonshik Han	(Seal)
Examiner	Sang-Kyu Ye	(Seal)
Examiner	Hyeong-Gon Moon	(Seal)
Examiner	Jeong Eon Lee	(Seal)

Abstract

NAD(P)-dependent steroid dehydrogenase-like (NSDHL) involved in breast tumor growth and metastasis has been implicated in the maintenance of cancer stem cells. However, its role in regulating breast cancer stem-like cells (BCSCs) remains unclear. This study aimed to uncover the molecular mechanisms by which NSDHL regulates the capacity of BCSCs. NSDHL knockdown suppressed tumor spheroid formation in estrogen receptor-positive (ER+) breast cancer cells grown on ultra-low-attachment plates. In RNA-sequencing analysis, as compared with control, 617 genes were found to be differentially expressed (fold change ≥ 2, $p \leq 0.05$) in NSDHL knockdown spheroids of MCF-7 cells, which associated with enriched TGFβ signaling pathway. In orthotopic tumor models injected with NSDHL-knockdown spheroids, tumor initiation and growth were strongly suppressed compared with those of the control. BCSC populations with CD44+/CD24- and CD49f+/EpCAM+ phenotypes and high ALDH activity were decreased in NSDHL-knockdown spheroids and xenograft tumors relative to controls, along with a decrease in the secretion of TGFβ

1 and 3, phosphorylation of Smad2/3, and expression of SOX2. A positive correlation between the expression of NSDHL and SOX2 is found in breast cancer specimens of patients. Our findings reveal that NSDHL plays an important role in maintaining the BCSC population and tumor-initiating capacity, suggesting that NSDHL is an attractive therapeutic target to eliminate BCSCs, thus preventing breast cancer initiation and progression.

Keyword : Breast cancer, NSDHL, TGFβ, Cancer stem cell, Cholesterol, Tumor spheroid

Student Number : 2020-36557

Table of Contents

List of Tables

List of Figures

I. Introduction

Breast cancer cells with CD44+, CD24low/−, EpCAM+, and CD49f+ surface markers and high ALDH activity have been considered to be progenitors and breast cancer stem−like cells (BCSCs), which cause tumor onset, resistance, recurrence, and metastasis [1−3]. The biological activities of cancer stem cells (CSCs), including BCSCs, are regulated by several stemness−related genes, such as SOX2, and NANOG and intracellular signaling pathways such as TGFβ/Smad [4].

Cholesterol accumulation is an accelerator of cancer development and progression in diverse cancers, including breast cancer [5, 6]. Cholesterol, its metabolites, and cholesterol biosynthesis genes have been recently established to play an essential role in several biological processes, including CD44 localization and TGFβ signaling, to support cancer stemness, tumor initiation, progression, and metastasis [7−16].

The genetic and pharmacological inhibition of cholesterol biosynthesis enzyme such as 3−hydroxy−3−methylglutaryl−coenzyme A reductase (HMGCR), farnesyl−diphosphate farnesyltransferase 1 (FDFT1), farnesyl pyrophosphate synthase (FDPS), and 24−dehydrocholesterol reductase (DHCR24) are

essential for propagating cancer stem cells and tumorigenesis [14, 17, 18]. The HMGCR inhibitor simvastatin induces downregulation of OCT4, SOX2, and NANOG in the human breast cancer cell line MCF-7 [19]. Consequently, cholesterol biosynthesis genes may represent intriguing targets for regulating the stemness of BCSCs.

NAD(P)-dependent steroid dehydrogenase-like (NSDHL) is an essential enzyme that catalyzes the $NAD(P)^+$-dependent oxidative decarboxylation of the C4 methyl groups of 4-alpha-carboxysterols in post-squalene cholesterol biosynthesis [20]. Lately, we reported for the first time that NSDHL regulates breast cancer cell proliferation and migration abilities, as well as tumor growth and metastasis, and is a poor prognostic biomarker in breast cancer patients [21]. However, the biological role of the NSDHL gene in the regulation of BCSC properties remains lacking.

Specially, cholesterol was directly implicated in the development of estrogen receptor-positive (ER+) breast cancer in mice [22] and pharmacological inhibitor of cholesterol biosynthesis was associated with a reduced risk of breast cancer recurrence in patients with ER+ breast cancer [23], suggesting the involvement of cholesterol biosynthesis genes in maintaining the BCSC population and tumor-initiating capacity. We aimed to investigate whether the NSDHL gene plays a role in maintaining BCSCs and

elucidate the molecular mechanism by which the NSDHL gene regulates BCSCs to drive tumorigenesis and tumor progression in ER+ breast cancer cells.

Herein, NSDHL knockdown inhibited BCSC-enriched tumor spheroid formation of ER+ human breast cancer cells (MCF-7, ZR-75-1, and BT-474) by small interfering RNA (siRNA) and short hairpin RNA (shRNA). NSDHL knockdown reduced BCSCs with CD44+, CD24-, EpCAM+, and CD49f+ surface markers, and high ALDH activity in MCF-7 cells grown as three-dimensional spheroids and orthotopic xenograft tumors. Mechanistically, NSDHL knockdown reduced the secretion of TGFβ1 and TGFβ3, which then decreased SMAD2/3 phosphorylation and SOX2, and NANOG expression. Overall, our study revealed a critical function of NSDHL in the maintenance of BCSCs and tumor-initiating capacity.

II. Materials and Methods

Cell lines and culture

ER+ breast cancer cell lines, MCF-7, ZR75-1, BT-474 were used. MCF-7 (ATCC® HTB-22) cells were obtained from the American Type Culture Collection (Manassas, VA, USA) in 2012–2013. ZR-75-1 (KCLB No. 21500) and BT-474 cells (KCLB No. 60062) were obtained from the Korean Cell Line Bank (Seoul, Korea). MCF-7 cells were grown in DMEM (WelGENE, Seoul, Korea) supplemented with 10% fetal bovine serum (FBS) (WelGENE) and 1% penicillin-streptomycin (10,000 U/ml) (Gibco, Carlsbad, CA, USA). ZR-75-1 and BT-474 cells were grown in RPMI 1640 (WelGENE) supplemented with 10% FBS and 1% penicillin-streptomycin (Gibco). All cells were maintained at 37℃ in a humidified atmosphere of 95% air and 5% CO_2.

Antibodies and drug

For western blot and immunohistochemistry, we used the following antibodies: β-actin (sc-47778), SOX2 (sc-365823) and NANOG (sc-293121) from Santa Cruz (CS, USA); NSDHL (ab190353), mCherry (ab167453), CD24 (ab202073), CD44 (ab6124), EpCAM (ab20160) and ALDH1A1 (ab227964) from Abcam (Cambridge,

UK); Smad2 (#5339), Smad3 (#9523), Phospho-Smad2 (Ser465/467) (#3108) and Phospho-Smad3 (Ser423/425) (#9520) from Cell Signaling (Beverly, MA, USA); CD49f (NBP1-85747) from Novus Biologicals (Centennial, CO, USA); FITC-conjugated CD24 (555427), PE-conjugated CD44 (550989), and APC-conjugated EpCAM (347200) from BD Biosciences (Mansfield, MA, USA); FITC-conjugated CD49f (313606) from Biolegend (San Diego, CA, USA). Lovastatin (MK-803) (Selleckchem, Houston, TX, USA) was used for the drug sensitivity test of the HMG-CoA reductase inhibitor.

siRNA transfection

NSDHL ON-TARGETplus SMART pool siRNA or ON-TARGETplus Nontargeting siRNA pool were obtained from Dharmacon (Lafayette, CO, USA). Briefly, 20 nM siRNA was diluted in Opti-MEM® I Reduced Serum Medium and mixed with Lipofectamine 2000 RNAiMAX Reagent (Thermo Fisher Scientific, Waltham, MA, USA). The mixture was added to the cells, followed by incubation for 48 h at 37℃ in a CO_2 incubator.

Short hairpin RNA lentiviral transduction

NSDHL-targeting shRNA lentiviral particles (shNSDHL) (LPP-

HSH103352-LVRU6MH-c-100) and control shRNA lentiviral particles (shCtrl) (LPP-CSHCTR001-LVRU6MH-025-C) were purchased from Genecopoeia (Rockville, MD, USA). MCF-7 cells were seeded in each well of a 24-well plate 24 h before viral infection and replaced with media containing 5 μg/ml polybrene® (sc-134220, Santa Cruz) and 2×10^6 TU of lentiviral particles. After 72 h, the transduced cells were selected with 100 μg/ml hygromycin B Gold (Invivogen, San Diego, CA, USA) for 7 days. Selected cells expressing mCherry were sorted using a FACSCalibur flow cytometer (BD Biosciences, Franklin Lakes, NJ, USA).

Three-dimensional spheroid culture

Non-adherent three-dimensional culture, or "spheroid formation assay," is widely used to assess the stemness potential of cancer cells. For spheroid formation, cells were seeded on an ultra-low attachment plate coated with polymer-X at a density of 2.5×10^5 cells/ml DMEM or RPMI 1640 (WelGENE) supplemented with 10% KnockOut™ Serum Replacement (Invitrogen, Carlsbad, CA, USA) and 1% penicillin-streptomycin (Gibco, Carlsbad, CA, USA). The culture medium was replaced every 3 days.

Quantification the spheroid size

Standalone image analysis software (ImageJ) was used in comparing the siCtrl and siNSDHL cellular quantification of the results. Twenty single spheroids per cell were analyzed in MCF-7, ZR-75-1 and BT-474 cells with ImageJ software. To quantify the spheroid area, the processed image was loaded into ImageJ (available as free software by http://rsbweb.nih.gov/ij/) and converted into a 8-bit image. After setting the scale to convert pixel numbers to standard units, the red channel of thresholding was adjusted and resulting thresholded images were binary and will only show the spheroid region. After segmentation, images were measured by providing the pixel size (0–infinity) and circularity (0.00–1.00). The ImageJ software separately clustered the cells without background noise and the spheroid sizes were calculated in each spheroid.

Quantitative reverse transcription-polymerase chain reaction (qRT-PCR)

Total RNA was extracted from cells using Tri-RNA reagent (FAVORGEN, Kaohsiung, Taiwan). qRT-PCR was conducted using a cDNA kit (Takara, Kusatsu, Shiga, Japan). Real-time PCR reactions were run on a Light Cycler 480 II (Roche, Salt Lake City,

UT, USA) using a SYBR Green PCR master mix (Applied Biosystems) and specific primers (Table 1). Results were analyzed using the $^{\Delta}$CT method or $2^{-\Delta\Delta}$CT method, which reflects the threshold difference between a target gene and GAPDH in each sample, as well as the relative gene expression, with the reference sample set to 1 (control).

Table 1. Specific primer sequences used for real-time RT-PCR

Gene	Sequence (5′->3′)	
NSDHL	Forward	GGTGACGCACAGTGGAAAAC
	Reverse	TCGCACGGACTCATTTGACA
HMGCR	Forward	GGGAACCTCGGCCTAATGAA
	Reverse	CACCACGCTCATGAGTTTCCA
PMVK	Forward	GCCTTTCTCTCCGCGTGTCT
	Reverse	GGAGCGGCAACAAGGAACA
SQLE	Forward	GCGTGCTTGGCTCTGCTTT
	Reverse	CCTGGGCATCAAGACCTTCCA
LSS	Forward	GCACTGGACGGGTGATTATGGT
	Reverse	CGCAGGTACCGCACAATCTCTT
CYP51A1	Forward	CAGGGATTGATCCGCCTCTTCA
	Reverse	CACAGAATGGGGCGGGATGTT
DHCR7	Forward	GGGGCCGGTTCAAGAAGGAAA
	Reverse	GCCCTTGAGATGCGGTTCTGT
Hu-Col4	Forward	AGGTGTTGACGGCTTACCTG
	Reverse	TTGAGTCCCGGTAGACCAAC
Hu-Col1	Forward	GTGATGCTGGTCCTGTTGGT
	Reverse	CACCATCGTGAGCCTTCTCT
ED-A	Forward	CCAGGTACAGGGTGACCTAC
	Reverse	CTCTCCATATCATCGTGCAA
ED-B	Forward	CGCTAAACTCTTCCACCATT
	Reverse	CCGCCATTAATGAGAGTGAT
IIICS	Forward	CCAGAGATCTTGGATGTTCC
	Reverse	GCCTAAAACCATGTTCCTCA
CD24	Forward	TCTAAATGTGGCTATTCTGTC
	Reverse	TATTTGGGAAGTGAAGACTGGA

CD44	Forward	TCCAACACCTCCCAGTATGA
	Reverse	GGCAGGTCTGTGATGT
ALDH1A1	Forward	TGTTAGCTGATGCCGACTTG
	Reverse	TTCTTAGCCCGCTCAACACT
ALDH1A2	Forward	CTGGCAATAGTTCGGCTCTCTC
	Reverse	TGATCCTGCAAACATGCTC
ALDH1A3	Forward	TCTCGACAAAGCCCTGAAGT
	Reverse	TATTCGGCCAAAGCGTATTC
OCT4	Forward	ACCGAGTGAGAGGCAACC
	Reverse	TGAGAAAGGAGACCCAGCAG
KLF4	Forward	TACCAAGAGCTCATGCCACC
	Reverse	TCATCTGAGCGGGCGAATTT
SOX2	Forward	CGAGTGGAAACTTTTGTCGGA
	Reverse	TGTGCAGCGCTCGCAG
NANOG	Forward	CTGCCGTCTCTGGCTATAGATAA
	Reverse	TACGAATACATCTTCATCACCAA
GAPDH	Forward	GAGTCCAGGGCGTCTTCA
	Reverse	GGGGTGCTAAGCAGTTGGT

RNA isolation and RNA-seq

Total RNA was extracted from BCCs using TRIzol reagent (Invitrogen) according to the manufacturer's instructions. RNA concentration was measured using a NanoDrop 2000 spectrophotometer (Thermo Fisher Scientific). The RNA integrity number was determined using an Agilent RNA 6000 Nano kit following the manufacturer's protocol on an Agilent 2100 bioanalyzer (Agilent, Santa Clara, CA, USA).

Sequencing libraries were constructed using a QuantSeq 3' mRNA-Seq Library Prep Kit (Lexogen, South Morang Victoria, Australia) according to the manufacturer's instructions. High-

throughput RNA-seq was performed by single-end 75-bp sequencing using a NextSeq 500 system (Illumina, San Diego, CA, USA). The differentially expressed genes (DEGs) between BPA-exposed BCCs and control cells were determined based on counts from unique and multiple alignments using coverage in BEDtools [24]. The read count data were processed based on the quantile normalization method using the EdgeR package within R using Bioconductor [25]. To select DEGs, we ranked genes with a *p*-value of <0.05, using the log10 p-value, and plotted them against the log2-fold change (FC) in a volcano plot. Upregulated and downregulated genes with *p*-values <0.05, and log2FC ratios >0.59 were identified.

Western blotting

Cells were lysed in RIPA buffer (Sigma, St. Louis, MO, USA). Proteins were separated using SDS-PAGE and transferred onto Immobilon-P Transfer membranes (Merck Millipore, Bedford, MA, USA). After blocking with 5% non-fat dry milk in TBS-T or 5% BSA in TBS-T at room temperature for 1 h, the membrane was incubated with primary antibodies overnight at 4℃ and horseradish peroxidase-conjugated secondary antibodies at room temperature for 1 h and visualized using SuperSignal West Pico

Chemiluminescent Substrate (Thermo Fisher Scientific) and Amersham Imager 600 (GE Healthcare, Buckinghamshire, UK). The relative intensities of the bands observed by western blotting were analyzed using ImageJ software (National Institutes of Health, Bethesda, MD, USA).

Bio-Plex Pro™ TGFβ immunoassays

TGFβ 1, 2, and 3 levels were determined using BioPlex Pro(TM) TGFβ Assay kits (Bio-Rad Laboratories, Inc., Hercules, CA, USA). Conditioned medium of spheroids cultured for 3 days was analyzed according to the manufacturer' s protocol. Fluorescence intensity was measured and data analysis was performed using the Bio-Plex200 multiplex array system and Bio-Plex Manager 5.0 (Bio-Rad).

Flow cytometry

Spheroids were digested with 0.25% trypsin, washed three times with PBS, followed by being re-suspended in 1%BSA/PBS, and then stained with antibodies (CD44-PE, CD24-FITC, EpCAM-APC, and CD49f-FITC), or stained with their isotype controls at room temperature for 20 min. Flow cytometry analysis was performed using a BD FACSCanto™ II Flow Cytometer (BD Bioscience). The

percentage of CD24+, CD44+, CD49f+, EpCAM+, CD44+/CD24−, or EpCAM+/CD49f+ subpopulations was calculated using flow cytometry.

Immunofluorescent staining

The spheroids were fixed with 4% paraformaldehyde, permeabilized in 1%BSA/PBS− Triton X−100 at 4℃, and incubated with primary antibodies (NSDHL [1:50], CD24, CD44 [1:10] and EpCAM, CD49f [1:20]) overnight at 4℃ and secondary antibodies (Alexa Fluor® 488 goat anti−rabbit IgG (H+L) [1:1000] at room temperature for 15 min, followed by incubation with NucBlue® Live REAdyProbes™ REAgent (Thermo Fisher Scientific). The cell images were acquired using a confocal microscope (Leica, Wetzlar, Germany).

ALDEFLUOR™ assay

The ALDEFLUOR reagent system (Stem Cell Technologies, Vancouver, Canada) was used to determine the ALDH1 activity of cells according to the manufacturer's protocol. Cells (1×10^6) dissociated from spheroids were suspended in the ALDEFLUOR™ Assay buffer containing the ALDH substrate, boron−dipyrromethene−aminoacetaldehyde (BAAA), and incubated for 40 min at 37℃. The negative control was treated with 50 mmol/L of an

ALDH-specific inhibitor, diethylaminobenzaldehyde (DEAB). Cells with high ALDH activity were analyzed using a FACSCalibur flow cytometer (BD Biosciences).

Total cholesterol assay

Total intracellular cholesterol levels in spheroids were measured using the Total Cholesterol Assay Kit (Cell Biolab, Inc., San Diego, CA, USA). Cholesterol standards and samples were prepared according to the manufacturer's instructions. A total of 25 μl of diluted cholesterol standards/serum samples and 25 μl of the cholesterol reaction reagent consisting of cholesterol esterase and cholesterol oxidase, fluorometric probe, and horseradish peroxidase were added to each well. After incubation for 45 min at 37℃, fluorescence signals were measured using a microplate reader (Synergy H1, BioTek Instruments, Inc., Winooski, VT, USA) at an excitation and emission wavelengths of 550 and 595 nm, respectively. The concentration of cholesterol in the samples was calculated by comparing the sample RFU to the cholesterol standard curve.

Xenograft animal model

NOD.Cg-Prkdc^{scid} Il2rg^{tm1wjl} /SzJ mice (NSG mice) were obtained from The Jackson Laboratory (Bar Harbor, ME, USA). All animal experiments were approved by the Institutional Animal Care and Use Committee of the Seoul National University (IACUC, SNU 200907-4). Forty female NSG mice were used in this study. Orthotopic xenografts were established by injecting $5\times10^2-1\times10^6$ cells of control shRNA (shCtrl)- or shRNA-targeting NSDHL (shNSDHL)-spheroids mixed with Matrigel (BD Biosciences) into the fat pad of the fourth mammary gland of 5-week old mice and allowed to drink water supplemented with β-estradiol (6.25 μg/ml). After injection of tumor cells, the primary tumor volume was measured weekly using digital calipers and a modified ellipsoidal formula (volume=1/2 [length×width^2]).

Immunohistochemistry

The primary tumors were fixed with 4% buffered paraformaldehyde, embedded in paraffin blocks, and sectioned into 4-μm thick sections. The sections were deparaffinized in xylene, rehydrated in a series of graded ethanol and water solutions, and pretreated by autoclaving at 98℃ for 20 min in citrate (pH 6.0) or 10 mM Tris/1 mM EDTA (pH 9.0) for antigen retrieval. Endogenous peroxidase

activity was blocked by incubation with 3% H_2O_2 for 10 min at room temperature. After incubation with 10% normal goat serum for 1 h to block nonspecific binding of immunological reagents, primary antibodies at 4℃ overnight and secondary antibodies were applied, and immunoreaction was visualized using the DAB chromogen kit (Agilent Technologies, Glostrup, Denmark). For double staining of ALDH1/CD44, the DoubleStain IHC Kit (ab183285) was used. Nuclei were counterstained with hematoxylin solution (Merck Millipore) according to the manufacturer's instructions. Histological images of the stained tissues were acquired using a microscope equipped with a CCD camera (Leica, Wetzlar, Germany).

Survival outcomes analysis of the NSDHL mRNA expression levels and correlation analysis of NSDHL, NANOG, and SOX2 expression in breast cancer patients

The relationship of NSDHL genes on relapse-free survival (RFS) and distant metastasis-free survival (DMFS) of breast cancer patients with a mean follow-up of 120 months was evaluated by the Kaplan–Meier Plotter (http://www.kmplot.com/analysis) surveyed public microarray data repositories. The cutoff value of NSDHL expression was chosen as median which split the patient samples into two groups and plots generated accordingly. ER+ or ER– status

was determined by both immunohistochemistry and array. Correlation between NSDHL, NANOG, and SOX2 expression of TCGA RNA-Seq results of patients with luminal type breast cancer was evaluated using Pairwise Spearman's rank correlation test.

Statistical analyses

In the analysis of data obtained in vitro and in vivo, graphs are presented as mean ± standard deviation of at least three independent experiments. Statistical comparisons between the two independent groups were performed using the unpaired t-tests. Data were analyzed using Kruskal-Wallis nonparametric ANOVA followed by the Dunn's multiple comparison test for groups of three or more. Statistical analyses were performed using GraphPad Prism v9.2.0 (GraphPad Software Inc., La Jolla, CA, USA). Statistical significance was set at $p < 0.05$, $0.001 < p < 0.05$, $p < 0.001$.

III. Results

NSDHL knockdown represses a tumor spheroid formation of ER+ breast cancer cells cultured on ultra-low attachment plate

In our previous study by using multivariate analysis to account for ER status, high NSDHL levels were shown to be independently associated with short survival [21]. Another investigation was conducted using the Kaplan-Meier Plotter database. The level of NSDHL mRNA in ER-pos and ER-neg patients using TCGA-RNA seq data, we found that NSDHL expression was higher in ER- patients (p<0.0001, Fig. 1a). In ER+ breast cancer patients, high expression of NSDHL was associated with worse RFS (n = 2561, HR = 1.22, 95% CI 1.04-1.43, p=0.014) and DMFS (n = 1109, HR = 1.32, 95% CI 0.99-1.75, p=0.055) (Fig. 1b,c). However, no significant difference existed between low and high NSDHL expressions in RFS (HR = 0.86, 95% CI 0.68-1.09, p = 0.22) and DMFS (HR = 1.09, 95% CI 0.8 -1.49, p = 0.57) of ER-breast cancer patients (Fig. 1d, e). These results suggest that NSDHL may serve as an important survival predictor in ER+ and be associated with an increased risk of relapse and distant metastasis of ER+ breast cancer cells. BCSCs are suggested to be response for breast cancer relapse and distant metastasis. Therefore, we investigated

the involvement of NSDHL in maintenance of BCSCs in ER+ breast cancer cells.

NSDHL levels and tumor spheroids were examined in the ER+ breast cancer cells MCF-7, BT-474, and ZR-75-1. In monolayer culture condition, NSDHL mRNA and protein levels were found to be greater in MCF-7 and BT-474 cells than in ZR-75-1 cells (Fig. 2a, b). Even after three days of growth, MCF-7 and BT-474 cells, but not ZR-75-1 cells produced cohesive and round tumor spheroids (Fig. 2c). The size and ability of the spheroid to form were found to be related to the degree of NSDHL expression. In MCF-7, ZR-75-1, and BT-474 cells, the biological effect of NSDHL knockdown by siRNAs on tumor spheroid formation was investigated. Introduction of siNSDHL significantly reduced the NSDHL mRNA and protein levels by ~0.5 and 0.9-fold in MCF-7, ZR-75-1, and BT-474 (p<0.0001, Fig. 3a, b). The spheroid size was observed in MCF-7 (from 25068.93±9662.49 μm2 to 7488.46±2421.47 μm2, p<0.0001), ZR-75-1 (from 39863.18 ± 13556.92 μm2 to 14886.38± 4625.96 μm2, p<0.0001), and BT-474 (from 97440.14± 83697.93 μm2 to 53604.94± 21108.88 μm2, p=0.03) cells and we found that NSDHL knockdown cells were decreased compared to control siRNA (siCtrl) cells (Fig. 3c). Thus, it could be speculated that the NSDHL expression could have

accelerated the tumor spheroid formation.

After 3 days of suspension culture, siNSDHL−MCF−7 spheroids were not tightly cohesive and circular aggregates, and had a distinct grape−like appearance compared to MCF−7 controls. (Fig. 3d). Immunofluorescent staining revealed a reduction in NSDHL expression in siNSDHL−MCF−7 spheroids compared to that in the control (Fig. 3e). Likewise, levels of NSDHL mRNA (0.10±0.08, $p<0.0001$) and proteins (0.03±0.01, $p<0.0001$) were significantly decreased in siNSDHL−MCF−7 spheroids compared to the control (Fig. 3a, f, g). The total cellular cholesterol levels of tumor spheroids were measured to examine the effect of NSDHL knockdown on cholesterol biosynthesis. NSDHL knockdown reduced the total cellular cholesterol levels from 30.55±1.33 μg/mg to 18.84±0.42 μg/mg ($p<0.001$) in MCF−7 spheroids cultured for 3 days (Fig. 4a). These results indicate that NSDHL plays an important role in generating tumor−spheroid and maintaining the total cellular cholesterol levels.

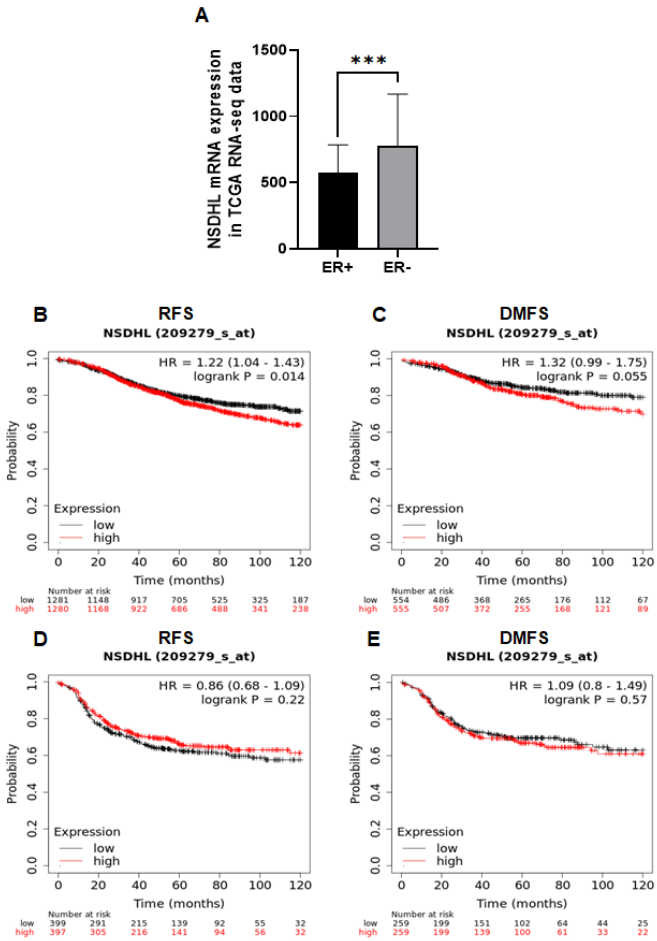

Figure 1. High NSDHL expression was associated with a shorter relapse-free survival (RFS) and distant metastasis-free survival (DMFS) in patients with ER+ breast cancer

a The level of NSDHL mRNA in ER-pos and ER-neg patients using TCGA-RNA seq data. b, c Association of NSDHL with survival outcomes in patients with ER+ breast cancer. d, e Association of NSDHL with survival outcomes in patients with ER- breast cancer. Analysis of Kaplan-Meier Plotter (http://www.kmplot.com) to

evaluate the effect of NSDHL mRNA on clinical outcomes of breast cancer patients with 120 months. ***p <0.001.

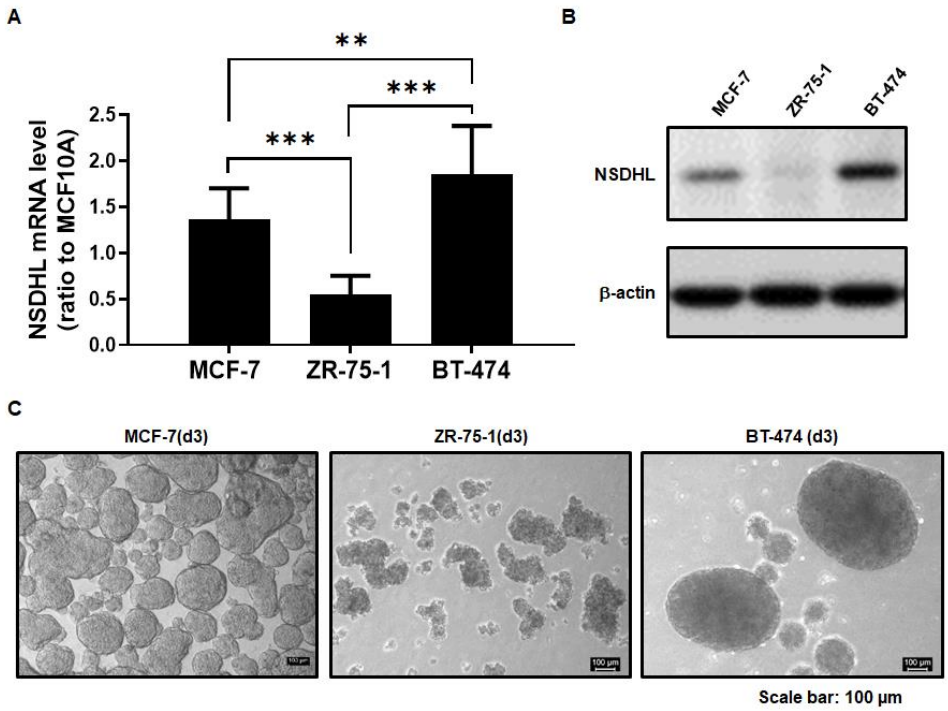

Figure 2. Analysis of NSDHL expression and spheroid formation in ER+ breast cancer cell lines MCF-7, ZR-75-1, BT-474.

a, b Relative NSDHL mRNA and protein levels were analyzed by real-time RT-PCR and western blot in luminal cell lines MCF-7, ZR-75-1 and BT-474. c Representative images of MCF-7, ZR-75-1, and BT-474 cells grown on ultra-low attachment plates. Data represent the mean ± standard deviation of three independent experiments. ** 0.001 < p <0.05, ***p <0.001.

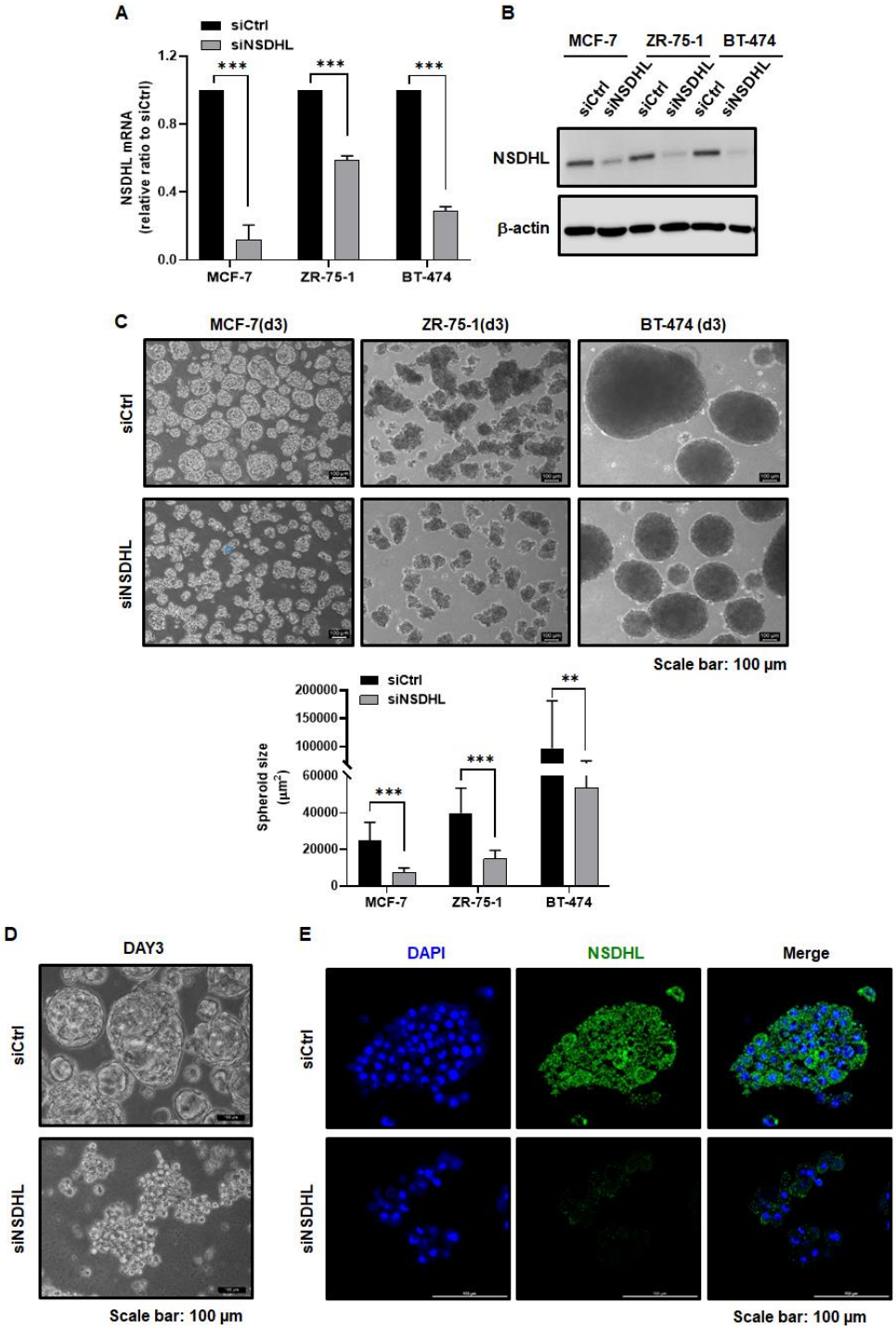
A
siCtrl
siNSDHL
NSDHL mRNA (relative ratio to siCtrl)
1.2
0.8
0.4
0.0
***
MCF-7
ZR-75-1
BT-474
B
MCF-7
ZR-75-1
BT-474
siCtrl
siNSDHL
NSDHL
β-actin
C
MCF-7(d3)
ZR-75-1(d3)
BT-474 (d3)
siCtrl
siNSDHL
Scale bar: 100 μm
Spheroid size (μm²)
200000
150000
100000
60000
40000
20000
0
**
D
DAY3
Scale bar: 100 μm
E
DAPI
NSDHL
Merge
Scale bar: 100 μm

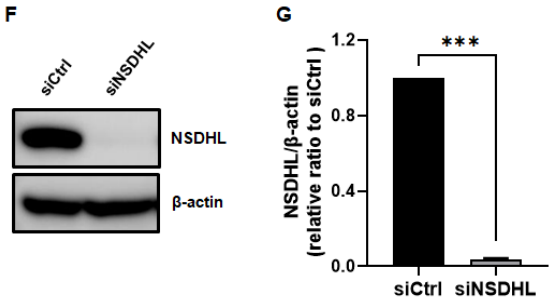

Figure 3. NSDHL knockdown represses a tumor spheroid formation of ER+ breast cancer cells, MCF-7, ZR-75-1, BT-474.

a, b Data of relative expression levels of NSDHL mRNA and protein levels in MCF-7, ZR-75-1, and BT-474 cells transfected with control (siCtrl)- or NSDHL siRNA (siNSDHL). c Representative images and quantification the size of spheroids of siCtrl- or siNSDHL-transfected MCF-7, ZR-75-1, and BT-474 cells grown on ultra-low attachment plates coated with polymer-X. d, e Representative images and immunofluorescence staining of DAPI (blue) and NSDHL (green) in spheroids of control (siCtrl)- or NSDHL siRNA (siNSDHL)-transfected MCF-7 cells cultivated on ultra-low attachment plates. f, g Protein levels of siNSDHL-spheroids relative to siCtrl-spheroids using western blot analysis. **$0.001<p<0.05$, ***$p<0.001$. Scale bar: 100 μm

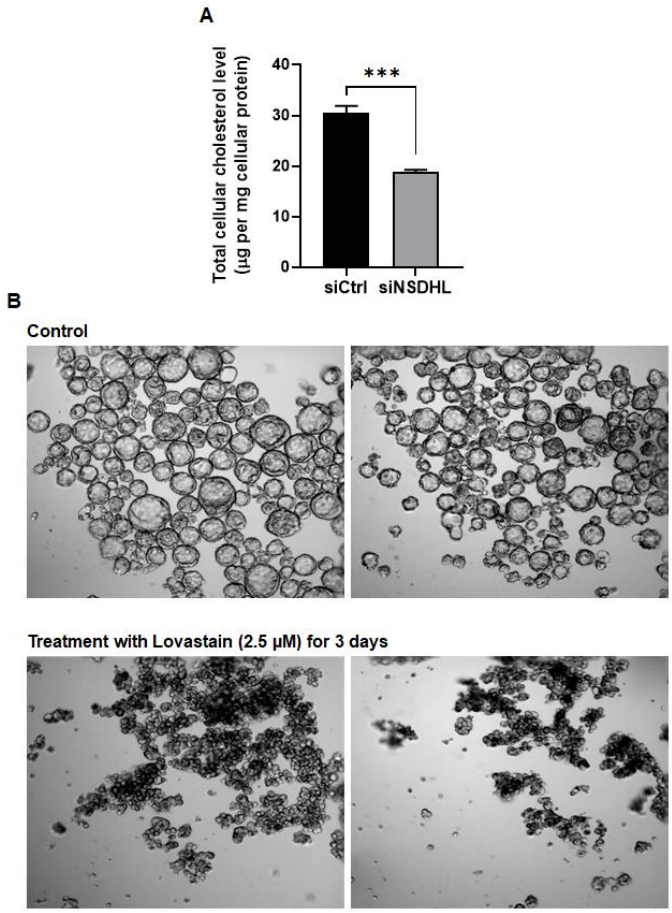

Figure 4. HMGCR inhibitor Lovastatin strongly suppressed the spheroid formation of MCF-7 cells.

a Total cholesterol levels measured in siNSDHL-spheroids and siCtrl-spheroids. b Representative images of spheroids of MCF-7 cells grown on ultra-low attachment plates in the presence or absence of lovastatin (2.5 μM) for 3 days. Data represent the mean ± standard deviations of five independent experiments. ***p <0.001

NSDHL knockdown decreases the BCSCs with CD44+/CD24− phenotype and high ALDH activity, and progenitors with EpCAM+/CD49f+ phenotype in tumor spheroids.

When compared to MCF−7 monolayers, MCF−7 spheroids upregulated the expressions of BCSC (CD44, ALDH1A1, ALDH1A2, and ALDH1A3), stemness (OCT4, KLF4, SOX2, NANOG), extracellular matrix (Col IV, FN−EDB, FN−EDA, and FN−IIICS)−related genes (Fig. 5a, b). Interestingly, we found that cholesterol synthesis genes (HMGCR, PMVK, SQLE, LSS, NSDHL, and DHCR7) were considerably elevated in MCF−7 spheroids compared to monolayers (Fig. 5c). NSDHL knockdown decreased the levels of HMGCR, PMVK, SQLE, and DHCR7 in MCF−7 spheroids (Fig. 5d). These finding suggests that cholesterol synthesis genes may be involved in enriching BCSCs (Fig. 5e).

In order to determine whether NSDHL knockdown impacts the BCSC and progenitor subpopulations with CD44+/CD24− and EpCAM+/CD49f+ phenotype, and high ALDH activity, flow cytometry and immunofluorescent staining were performed. CD44+ cells (from 42.8±17.27% to 11.9±6.24%, p=0.043), EpCAM+ cells (from 99.5±0.35% to 97.3±1.05%, p=0.025), and CD49f+ cells (from 1.5±1.0% to 0.47±0.31%, p=0.16) in MCF−7 spheroids decreased by NSDHL knockdown (Fig. 6a, b).

CD44+/CD24− BCSCs (from 0.63±0.15% to 0.1±0.08%, p=0.0018) as well as EpCAM+/CD49f+ progenitors (from 5.67±1.19% to 3.17±1.01%, p=0.05) in MCF−7 spheroids decreased by NSDHL knockdown (Fig. 6c, d). Likewise, immunofluorescence double staining showed that NSDHL knockdown led to a reduction in CD44+/CD24− and EpCAM+/CD49f+ cells (Fig. 6e). BCSC in MCF−7 spheroids, identified by high levels of ALDH activity also reduced by NSDHL knockdown (from 3.3±0.08% to 1.33±0.38%, p<0.0001, Fig. 6f, g). These data indicate that the NSDHL gene may play an important role in maintaining BSCSs.

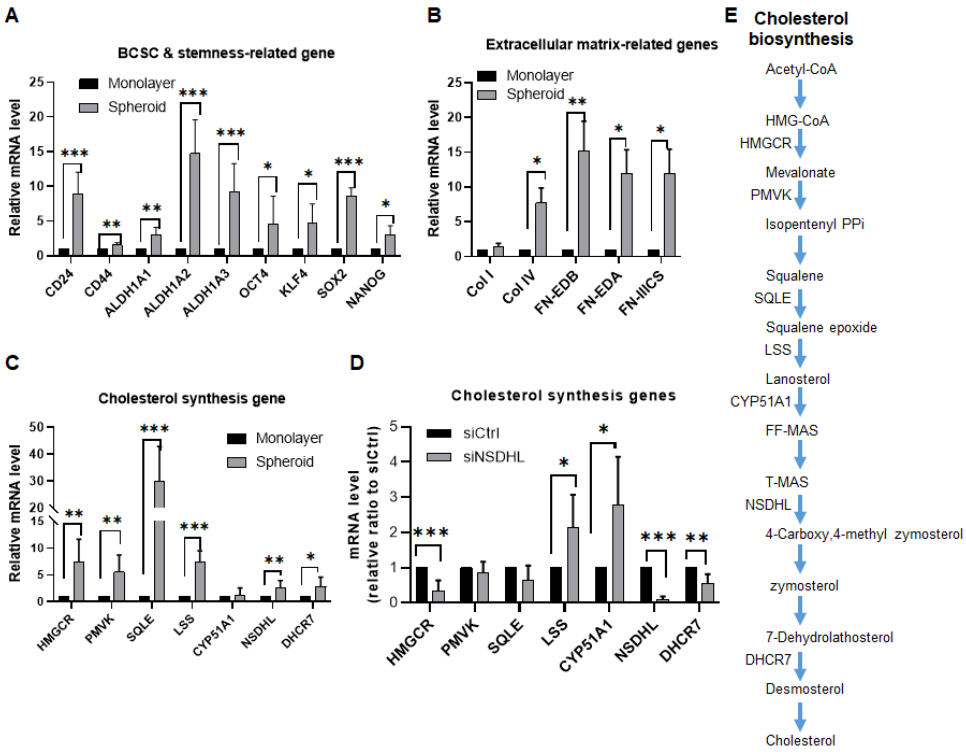

Figure 5. Relative mRNA expression levels of BCSC, stemness-related genes, extracellular matrix-related genes and cholesterol synthesis genes.

a-c Relative mRNA levels of BCSC and stemness-related genes (CD24, CD44, ALDH1A1, ALDH1A2, ALDH1A3, OCT4, KLF4, SOX2, and NANOG), extracellular-matrix-related genes (COLI, COLIV, FN-EDB, FN-EDA, and FN-IIICS), and cholesterol synthesis genes (HMGCR, PMVK, SQLE, LSS, CYP51A1, NSDHL, and DHCR7) assessed by qRT-PCR analysis in monolayer and spheroids. d Relative mRNA levels of cholesterol synthesis genes (HMGCR, PMVK, SQLE, LESS, CYP51A1, NSDHL, and DHCR7)

assessed by qRT−PCR analysis in siNSDHL−spheroids and siCtrl−spheroids. e Schematic related with NSDHL and cholesterol synthesis genes. Data represent the mean ± standard deviations of five independent experiments. $*p<0.05$, $**0.001<p<0.05$, $***p<0.001$.

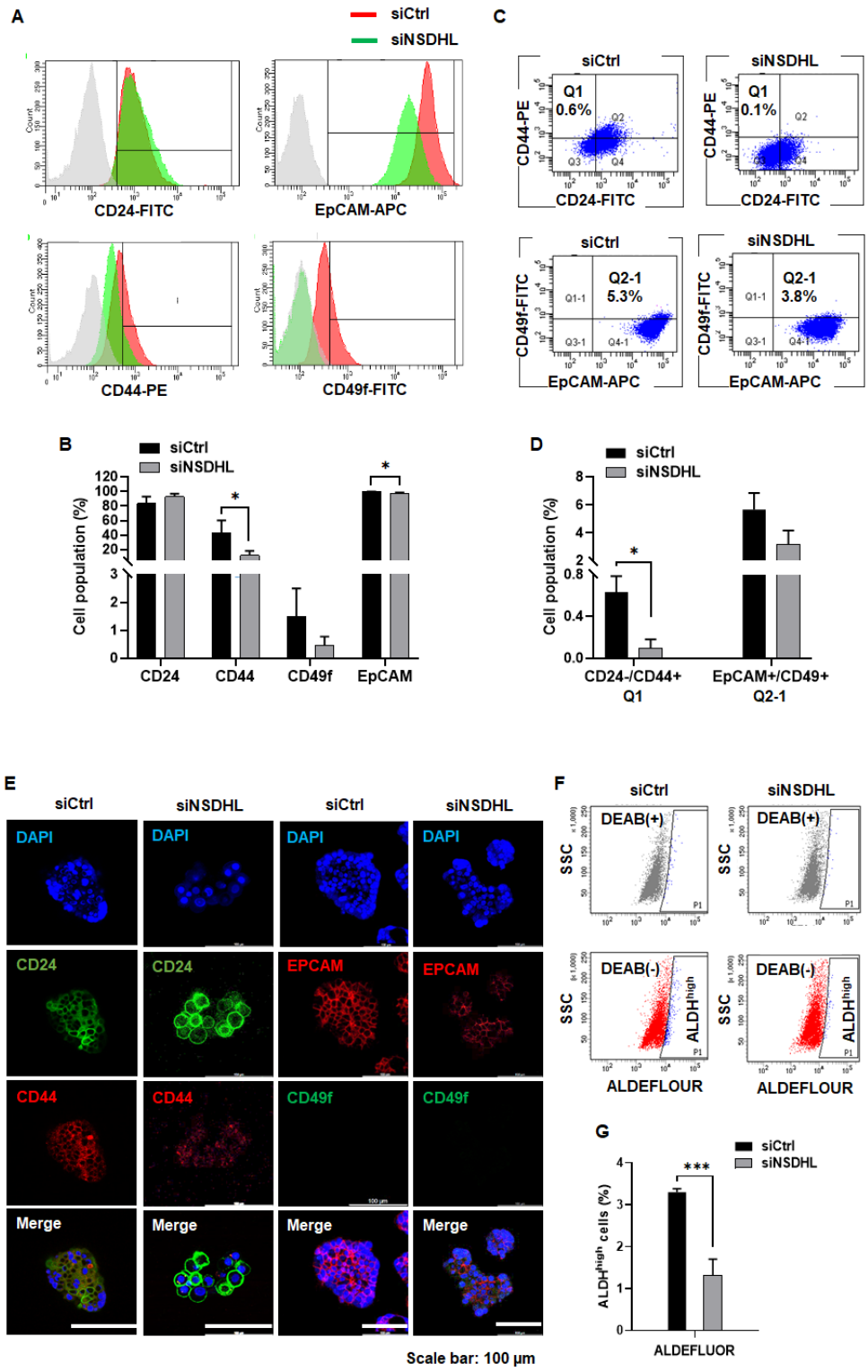
A
siCtrl
siNSDHL
CD24-FITC
EpCAM-APC
CD44-PE
CD49f-FITC
C
siCtrl
siNSDHL
Q1
0.6%
Q1
0.1%
CD44-PE
CD24-FITC
Q2-1
5.3%
Q2-1
3.8%
CD49f-FITC
EpCAM-APC
B
Cell population (%)
CD24
CD44
CD49f
EpCAM
D
CD24-/CD44+
Q1
EpCAM+/CD49+
Q2-1
E
DAPI
CD24
EPCAM
CD44
CD49f
Merge
Scale bar: 100 μm
F
DEAB(+)
DEAB(-)
SSC
ALDEFLOUR
G
ALDH^high cells (%)
ALDEFLUOR

Figure 6. NSDHL knockdown reduces the BCSCs with CD44+/CD24− phenotype and high ALDH activity, and progenitors with EpCAM+/CD49f+ phenotype in tumor spheroids

a, b Representative flow cytometry histograms and quantification of CD44+, CD24+, CD49f+, or EpCAM+ cells in control (siCtrl) and NSDHL siRNA (siNSDHL)−transfected MCF−7 spheroids. **c, d** Representative flow cytometry dot plots and quantification of CD44+/CD24− and EpCAM+/CD49f+ cells in siCtrl− and siNSDHL−spheroids. **e** Representative double immunofluorescence images of CD44+/CD24− and EpCAM+/CD49f− cells in siCtrl− and siNSDHL−spheroids. CD24 and CD49f (green), CD44 and EpCAM (red), DAPI (blue) **f, g** Representative flow cytometry dot plots and quantification of ALDH+ cells in siCtrl and siNSDHL−spheroids using the ALDEFLUOR assay. Data represent the mean ± standard deviation of three independent experiments. $*p < 0.05$, $***p < 0.001$. Scale bar: 100 μm

RNA-sequencing analysis reveals that NSDHL knockdown elicits widespread transcriptional changes

We performed RNA-sequencing (RNA-Seq) to identify the transcriptional targets of NSDHL and the mechanism of the effects of NSDHL knockdown on MCF-7 spheroids. Transcripts that were differentially regulated by log2 fold change>1 and $p<0.05$, are highlighted in red or green (Fig. 7a, b). Comparison of siNSDHL spheroids with control showed 253-upregulation and 364-downregulation of differentially expressed genes (DEGs) (Fig. 7c). The Kyoto Encyclopedia of Genes and Genomes (KEGG) pathway analysis was performed to understand the biological functions and interactions of genes modulated by NSDHL knockdown. The top 10 enriched KEGG pathways of upregulated DEGs gene sets are shown in figure 7d. The most enriched KEGG pathway terms with the highest levels of gene representation were TGFβ signaling pathway, suggesting that NSDHL knockdown may alter TGFβ signaling and lead to a change in the characteristics of tumor spheroids, including stemness and tumorigenesis.

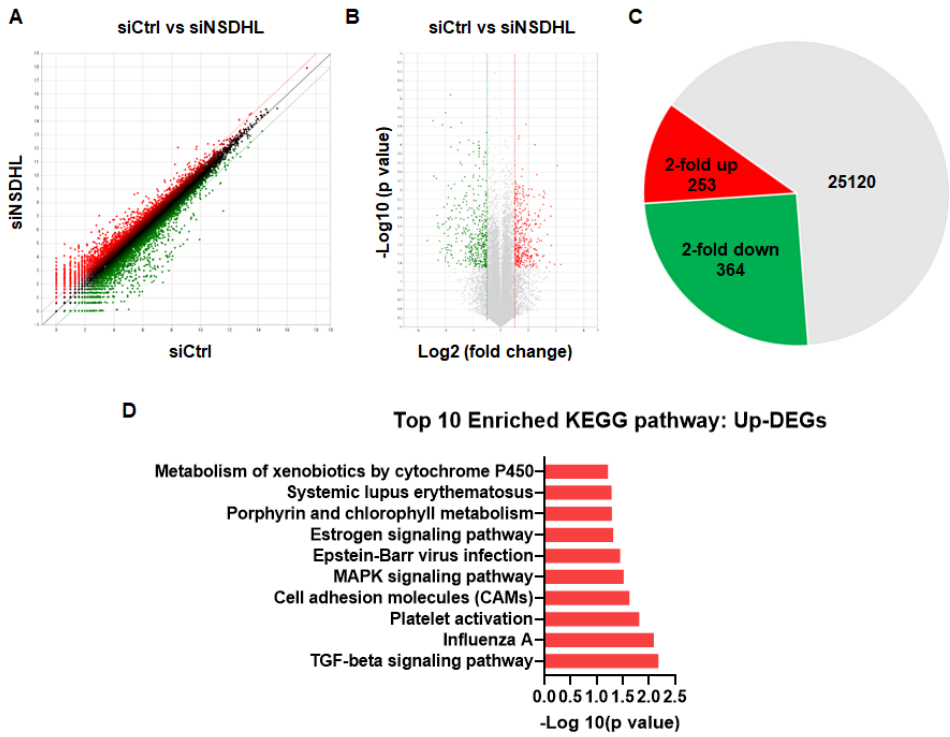

Figure 7. NSDHL knockdown leads to de-regulation of general gene expression associated with TGFβ signaling pathway, Cell adhesion molecules, and cell cycles

a, b, c Scatter plot, Volcano plot, and Venn diagram of differentially expressed genes (DEGs) comparing NSDHL siRNA (siNSDHL) and control siRNA (siCtrl)-transfected MCF-7 spheroids. d Top 10 enriched KEGG pathway analyses of DEGs.

NSDHL knockdown decreases the secretion of TGFβ 1 and 3, phosphorylation of Smad2 and 3, and expression of SOX2, and NANOG in tumor spheroids

Based on KEGG pathway analysis of RNA-seq data, we further explored the molecular mechanism by which NSDHL regulates BSCSs in tumor spheroids. To assess whether blocking TGFβ-Smad signaling can affect tumor spheroid formation, we treated MCF7 spheroids with A potent inhibitor of TGF-β type I receptor A-83-01 (50 μM). Spheroids treated with A-83-01 appeared less cohesive and exhibited the reduced phosphorylation of Smad 2 and Smad 3, which are canonical effectors of TGFβ signaling (Fig. 8a, b). A significant reduction in secreted levels of TGFβ 1 (2088.97±210.04 pg/ml vs 1542.46±373.41 pg/ml, p=0.01) and TGFβ 3 (60.13±8.09 pg/ml vs 23.3±8.56 pg/ml, p<0.0001) was detected in NSDHL knockdown spheroids relative to control (Fig. 8c). The phosphorylation of Smad2 (0.70±0.12, p<0.0001) and Smad 3 (0.63±0.15, p=0.0002), was significantly decreased by NSDHL knockdown as compared to the control (Fig. 8d-g).

Stemness-related genes such as SOX2, and NANOG, which have been reported to regulate CSC properties in a wide range of cancers, were examined. NSDHL knockdown led to marked reductions in

protein levels of SOX2 (0.62±0.13, $p<0.0001$), and NANOG (0.73±0.16, $p=0.0141$) as compared to those of the control (Fig. 8h-k). Similarly, qRT-PCR analysis revealed that the levels of SOX2, and NANOG mRNA were significantly decreased by NSDHL knockdown (Fig. 8l). These data suggest that a reduction in secreted levels of TGFβ 1 and TGFβ 3 results in a decrease in the phosphorylation of Smad2 and 3 and protein levels of SOX2, and NANOG, consequently leading to suppressed stemness of BCSC-enriched tumor spheroids.

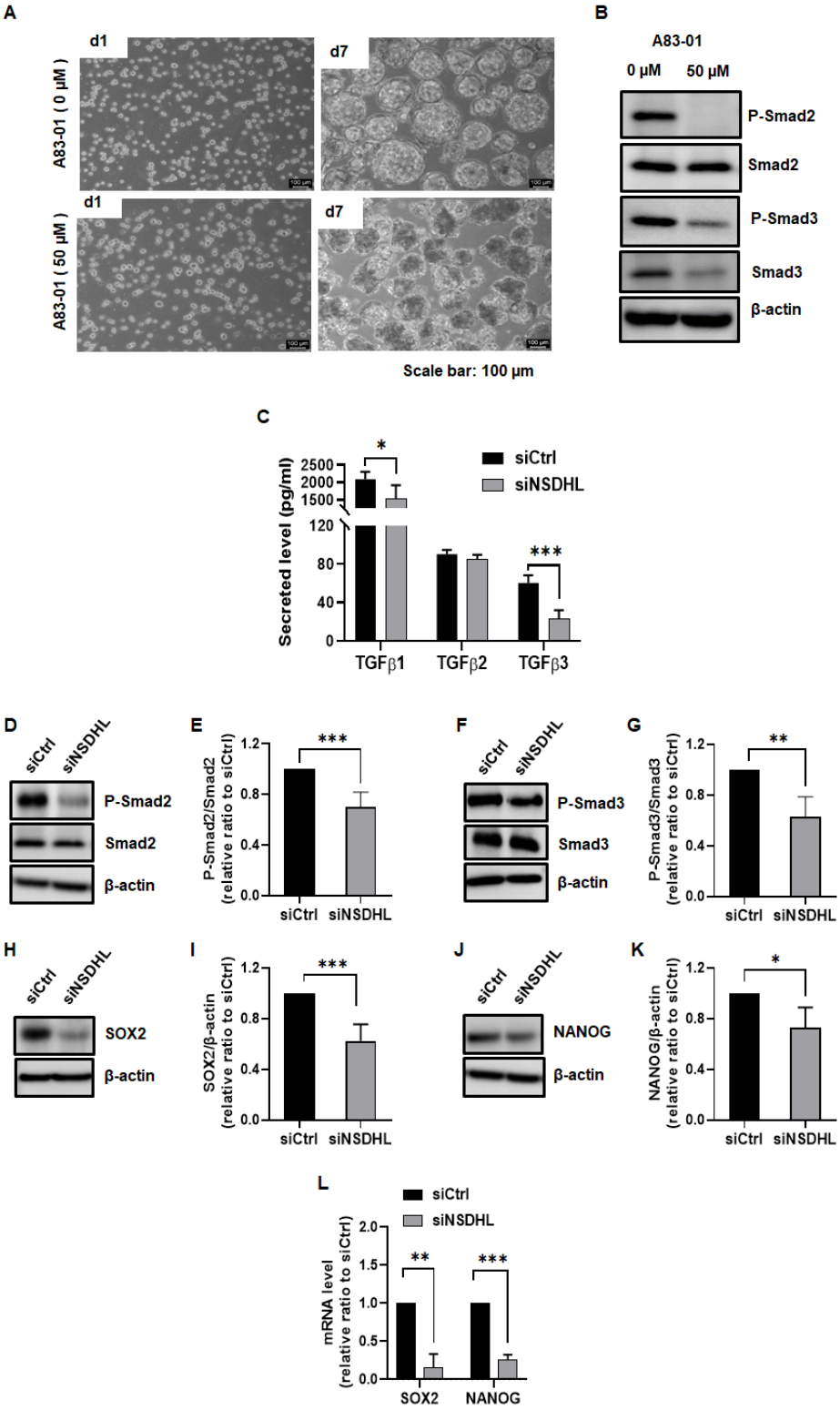
A
d1
d7
A83-01 (0 μM)
A83-01 (50 μM)
Scale bar: 100 μm
B
A83-01
0 μM
50 μM
P-Smad2
Smad2
P-Smad3
Smad3
β-actin
C
Secreted level (pg/ml)
siCtrl
siNSDHL
TGFβ1
TGFβ2
TGFβ3
D
E
P-Smad2/Smad2 (relative ratio to siCtrl)
F
P-Smad3
G
P-Smad3/Smad3 (relative ratio to siCtrl)
H
SOX2
I
SOX2/β-actin (relative ratio to siCtrl)
J
NANOG
K
NANOG/β-actin (relative ratio to siCtrl)
L
mRNA level (relative ratio to siCtrl)
SOX2
NANOG

Figure 8. NSDHL knockdown leads to a significant reduction in the secretion of TGFβ 1 and 3, phosphorylation of Smad2 and 3, and expression of SOX2 and NANOG in tumor spheroids

a, b Representative images of MCF-7 spheroids and western blot images of phopho-Smad2 and 3, Smad2, and Smad3 in the presence or absence of A-83-01 (50 μM) for 7 days. **c** Immunoassays of secreted TGFβ1, 2, and 3 levels measured from conditioned medium of siNSDH- or siCtrl-spheroids. **d-k** Representative western blot images and quantification data of phopho-Smad2 and 3, Smad2, Smad3, SOX2, and NANOG in siNSDH-spheroids relative to siCtrl-spheroids. **l** Relative mRNA levels of SOX2 and NANOG assessed by qRT-PCR analysis in siNSDHL-spheroids and siCtrl-spheroids. Data represent the mean ± standard deviation of six independent experiments. $*p < 0.05$, $** 0.001 < p < 0.05$, $***p < 0.001$

NSDHL knockdown represses tumorigenic potential of BCSC-enriched spheroids in the xenograft tumor model.

mCherry-positive cells in MCF-7 cells stably expressing control shRNA (shCtrl) or shRNA-targeting NSDHL (shNSDHL) were sorted by 99% (Fig. 9a, e). NSDHL shRNA transduction effectively reduced NSDHL mRNA and proteins levels by 0.06±0.01 and 0.25±0.07 respectively (p<0.0001, Fig. 9b-d). CD24- cells (from 66.27±5.94 to 72.30±10.00%, p=0.420), CD44+ cells (from 1.10±0.00% to 0.33±0.12%, p=0.0003) in MCF-7 spheroids decreased by NSDHL knockdown (Fig. 10a, b). Also we identified the high levels of ALDH activity also reduced by NSDHL knockdown (from 2.90±0.40% to 1.90±0.26%, p=0.022, Fig. 10c, d). We transplanted various concentrations of cells into the mammary fat pads of mice to evaluate the role of NSDHL in the in vivo tumorigenic potential. As shown in Table 2, shCtrl spheroids induced tumor formation within 30 days, even when as few as 500 cells per mouse were injected, whereas shNSDHL spheroids failed to induce tumor formation when <500 cells were injected, suggesting that NSDHL is responsible for the tumorigenic potential of BCSC-enriched spheroids. NSDHL knockdown significantly suppressed tumor volume at 49 days and 56 days post-injection (shCtrl vs shNSDHL; 527.79±270.95 and 232.09±113.86 mm3,

p=0.033 and 733.06±405.53 and 270.04±152.20 mm3, p=0.026, respectively), as measured with a caliper every 7 days (Fig. 11a) and induced significantly decreased tumor weights isolated from mice at 56 days at 7 days post-injection (shCtrl vs shNSDHL; 0.34±0.21 g and 0.13±0.08 g, p=0.043) (Fig. 11b, c). NSDHL shRNA transduction reduced NSDHL proteins levels by 0.39±0.33 (p=0.0013, Fig. 11d, e). The intensity of NSDHL immunohistochemical staining decreased in shNSDHL tumors compared with that in shCtrl tumors (Fig. 11f). These results suggest that NSDHL is responsible for tumor initiation and growth in vivo.

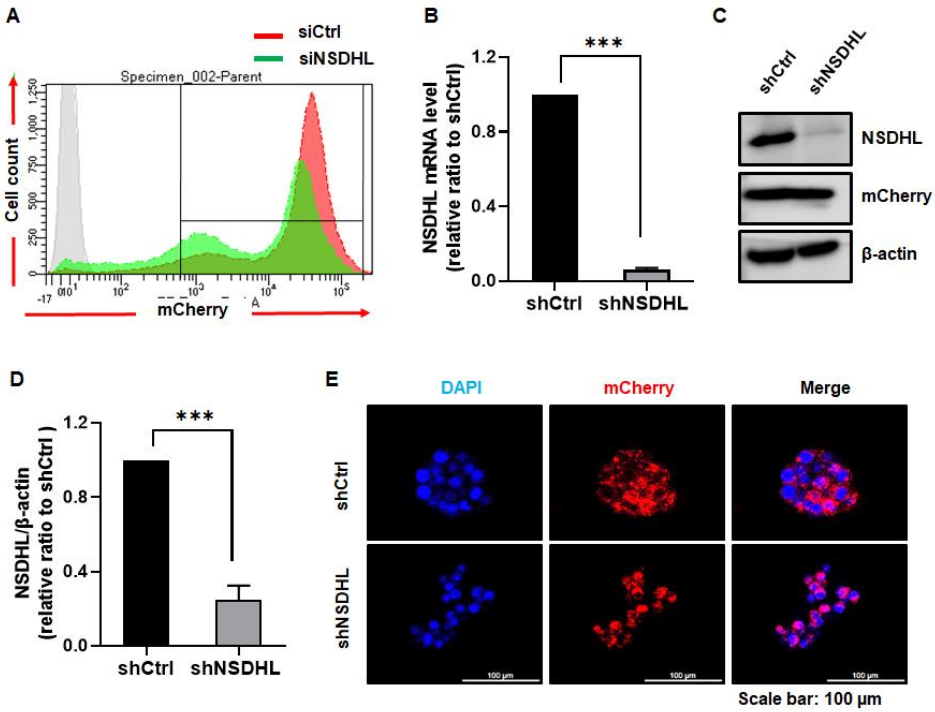

Figure 9. shCtrl and shNSDHL interacts with mCherry and is required for expression of mCherry.

a Representative flow cytometry histograms of mCherry-positive cells sorted from NSDHL shRNA (shNSDHL)- or control shRNA (shCtrl)-tagged mCherry-transduced MCF-7 cells. **b, c, d** NSDHL mRNA and protein levels and representative western blot images of NSDHL and mCherry in shNSDHL-spheroids relative to shCtrl-spheroids using qRT-PCR and western blot analysis. **e** Representative confocal images of mCherry-positive cells in shNSDHL- or shCtrl-spheroids. mCherry (red), DAPI (blue). Scale bar: 100 μm. Data represent the mean ± standard deviation

of six mice per group. ***p <0.001.

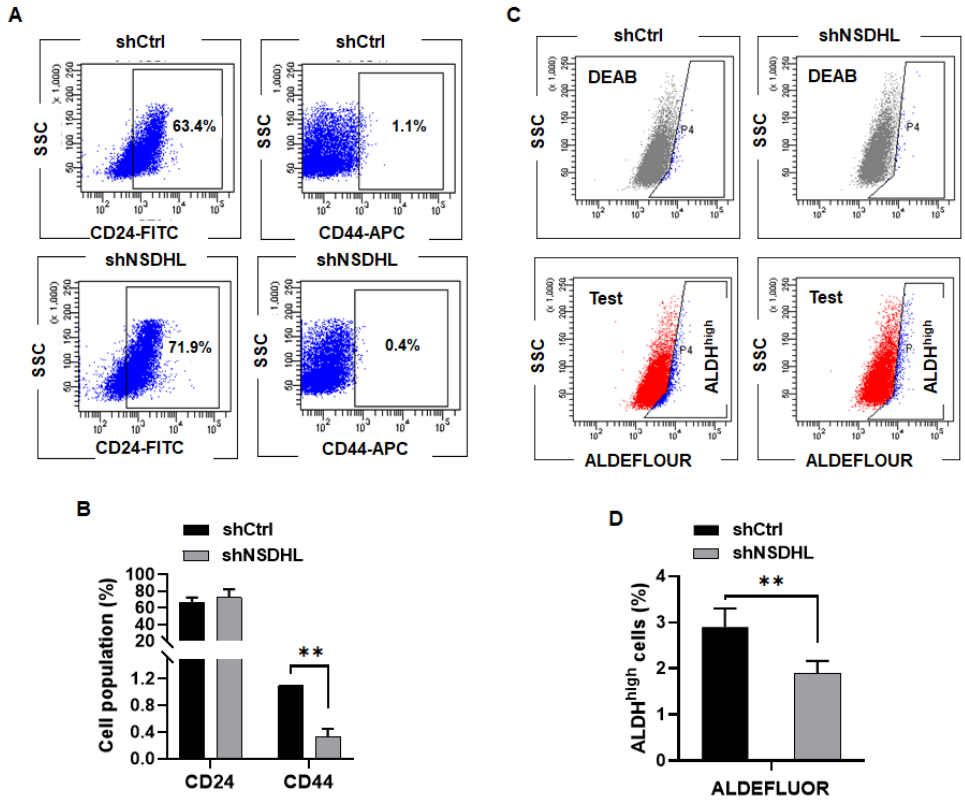

Figure 10. shNSDHL reduces CD44+ populations and ALDH activity.

a, b Representative flow cytometry dot plots and quantification of CD44+ and CD24− cells in control (shCtrl) and NSDHL shRNA (shNSDHL)−transduced MCF−7 spheroids. c, d Representative flow cytometry dot plots and quantification of ALDH+ cells in shCtrl− and shNSDHL−spheroids using the ALDEFLUOR assay. Data represent the mean ± standard deviation of five tumors per group. ** 0.001 < p <0.05

Table 2. Incidence of palpable tumor in mice injected with shCtrl or shNSDHL cells

Cell dose	Palpable tumor (%)		Termination (day)
	shCtrl group	shNSDHL group	
$5x10^2$	60% (3/5)	0% (0/5)	30
$5x10^3$	80% (4/5)	20% (1/5)	30
$5x10^4$	100% (5/5)	60% (3/5)	30
$1x10^6$	100% (6/6)	83% (5/6)	30

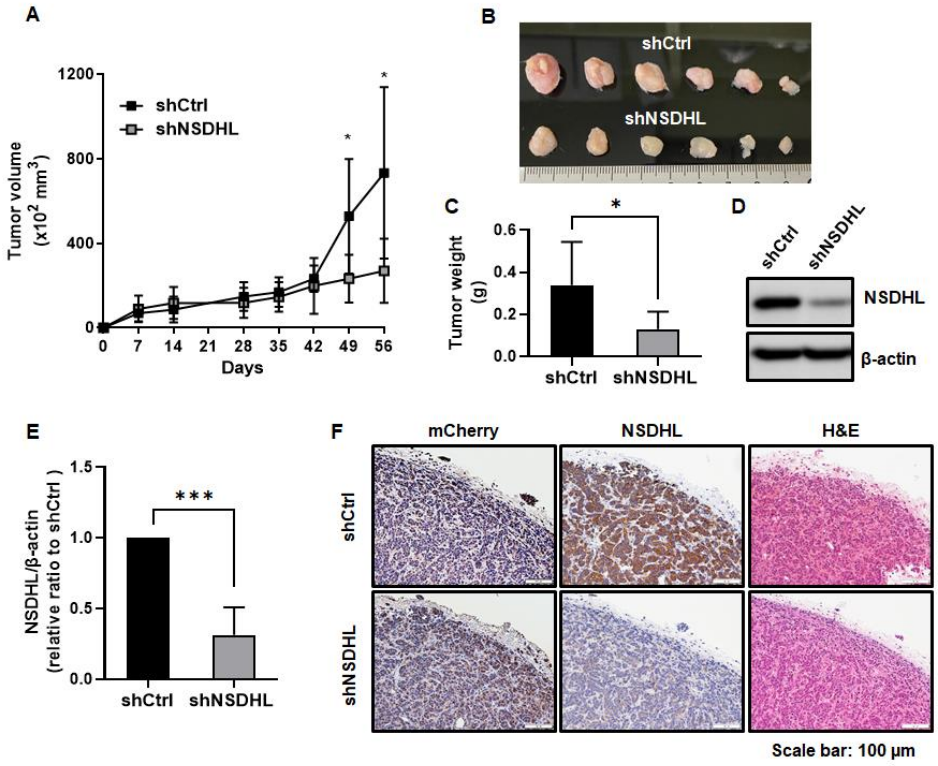

Figure 11. NSDHL knockdown suppresses tumor initiation and growth in xenograft tumor models

a Tumor volume data measured weekly in shNSDHL− or shCtrl−spheroid−injected mice during 56 days post−injection. **b, c** Gross images and wet weight of tumors removed from shNSDHL− or shCtrl−spheroid−injected mice at 56 days post−injection. **d, e** Representative western blot images and quantification data of NSDHL proteins in shNSDH−tumors relative to shCtrl−tumors. **f** Representative NSDHL and mCherry immunohistochemistry images and H&E images of shNSDHL− or shCtrl−tumor tissues. Scale bar: 100 μm. Data represent the mean ± standard deviation of six mice per group. $*p < 0.05$, $***p < 0.001$.

NSDHL knockdown caused a reduction in BCSCs with CD24−/CD44+ phenotype and high ALDH activity in a xenograft tumor model, accompanied by a significant decrease in Smad2/3 phosphorylation.

BSCS subpopulations with CD44+/CD24− phenotype or high ALDH activity were analyzed to verify the role of NSDHL in maintaining the BCSC population within tumors. Single stained CD24− and CD44+ cells of shCtrl and shNSDHL tumors were 3.66±1.17% and 1.35±0.41%, respectively (p=0.007, Fig. 12a, b), CD44+/CD24− cells decreased in shNSDHL tumors (0.5±0.37%) relative to shCtrl tumors (1.24±0.77%) (p=0.121, Fig. 12c, d). BCSCs with high ALDH activity in tumors, as assessed by ALDEFLUOR assay, were also reduced in shNSDHL tumors (0.88±0.29%) relative to shCtrl tumors (1.34±0.83%) (p=0.332, Fig. 12e, f). Double immunohistochemical staining showed a small subpopulation of CD44+/ALDH+ cells in xenograft tumors. NSDHL knockdown also led to a reduction in CD44+/ALDH+ cells within tumor tissues (Fig. 12g). In accordance with findings of in vitro spheroids, the levels of phosphorylated Smad2 (0.76±0.21, p<0.032), phosphorylated Smad3 (0.70±0.16, p=0.003) and SOX2 (0.76±0.30, p=0.12) were reduced in shNSDHL tumors relative to shCtrl tumors (Fig. 12h−m). Unlike what was expected from the results of spheroids, NANOG (1.19±0.68, p=0.68, Fig. 12n, o) was not decreased in

shNSDHL tumors relative to shCtrl tumors. This suggests that NSDHL knockdown leads to downregulation of Smad2 and Smad3 which are part of the TGFβ/Smad signaling cascade, and impair self-renewal capacity and tumorigenic potential of CD44+/ALDH+ cells.

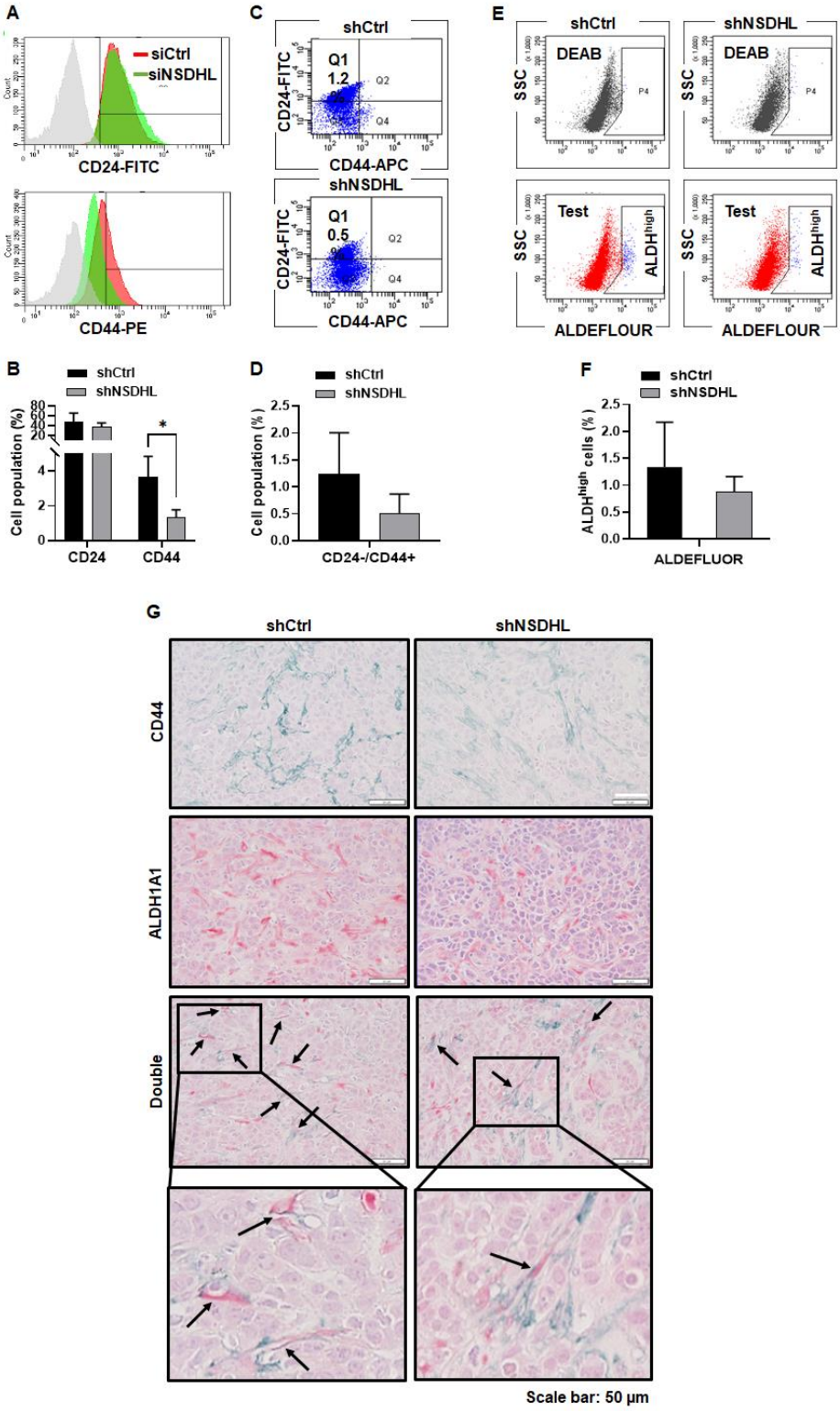
A
siCtrl
siNSDHL
CD24-FITC
CD44-PE
C
shCtrl
Q1
1.2
Q2
Q4
CD24-FITC
CD44-APC
shNSDHL
Q1
0.5
Q2
Q4
CD24-FITC
CD44-APC
E
shCtrl
shNSDHL
DEAB
P4
SSC
Test
ALDH^high
ALDEFLOUR
B
shCtrl
shNSDHL
Cell population (%)
CD24
CD44
D
shCtrl
shNSDHL
Cell population (%)
CD24-/CD44+
F
shCtrl
shNSDHL
ALDH^high cells (%)
ALDEFLUOR
G
shCtrl
shNSDHL
CD44
ALDH1A1
Double
Scale bar: 50 μm

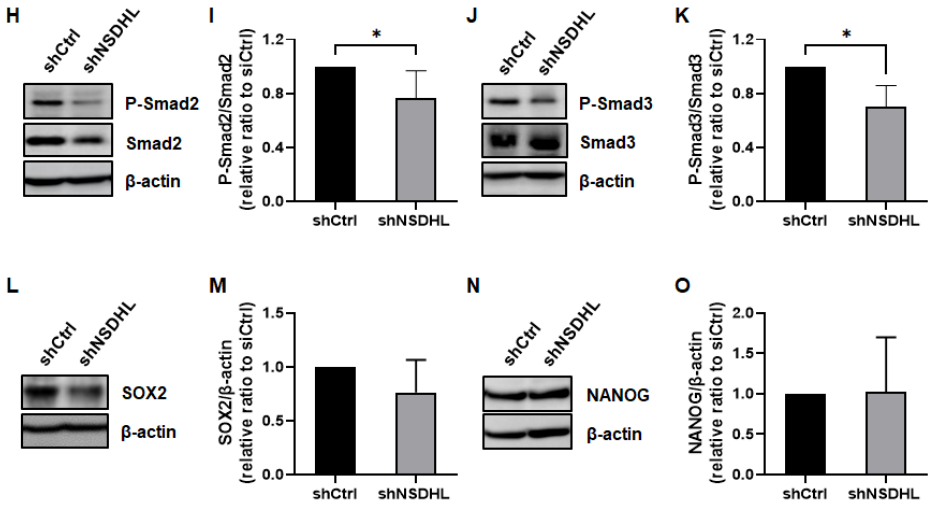

Figure 12. NSDHL knockdown reduces BCSC population with CD44+/CD24− phenotype and ALDH activity in xenograft tumor, accompanied by decreased Smad2/3 phosphorylation and NANOG expression

a−d Representative flow cytometry histograms and dot plots and quantification of CD44+ and CD24− cells in control (shCtrl) and NSDHL shRNA (shNSDHL)−transduced MCF−7 tumors. **e, f** Representative flow cytometry dot plots and quantification of ALDH+ cells in shCtrl− and shNSDHL−tumors using the ALDEFLUOR assay. **g** Representative double immunohistochemistry images of CD44+ and ALDH1A1+ cells in shCtrl− and shNSDHL−tumors. CD44 (green), ALDH1A1(red). Double CD44+/ALDH1A1+ cells (arrow). **h−o** Representative western blot images and quantification data of phopho−Smad2 and 3, Smad2, Smad3, SOX2,

and NANOG in shNSDHL-tumors relative to shCtrl tumors; data represent the mean ± standard deviation of five tumors per group. $*p < 0.05$

A positive correlation between the expression of NSDHL and SOX2 is found in breast cancer specimens of patients

To determine whether there were any correlations between NSDHL and BCSC-related genes in specimens of patients with luminal type breast cancer, we analyzed the expression levels of NSDHL and BCSC-related genes SOX2, and NANOG obtained from RNA-seq of breast tumor tissues (N=998) based on the TCGA database. Spearman's correlation analysis was used to evaluate the relationship among NSDHL, SOX2, and NANOG expression levels. Analysis based on the Spearman's correlation coefficient indicated a very week positive correlation between NSDHL and SOX2 gene expression in patient tumor tissue (r=0.089, p=0.005, Fig. 13a), whereas negative correlation was found between NSDHL and NANOG gene expression (r=0.038, p=0.24, Fig. 13b). The results of this study suggest coregulation or synchronized biological functions between NSDHL and SOX2.

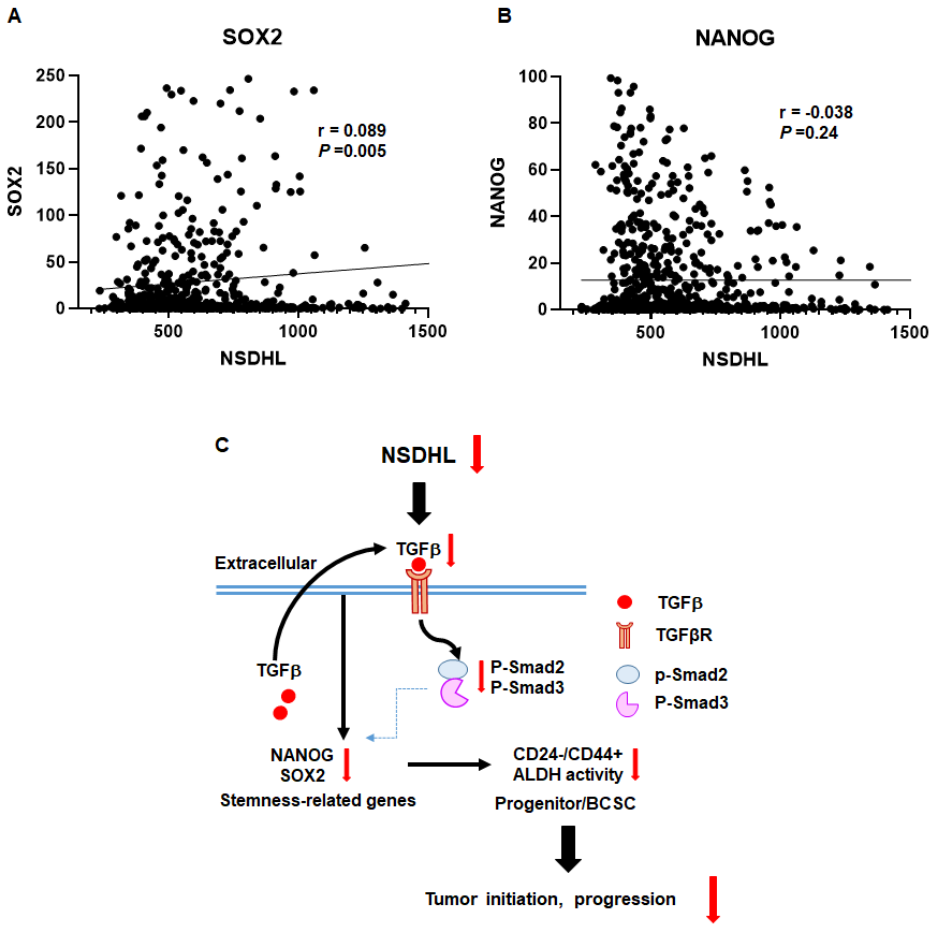

Figure 13. A positive correlation between NSDHL and SOX2 gene expression is found in tumor tissue of breast cancer patients

a, b Analysis of correlation among NSDHL, SOX2, and NANOG gene expression obtained from RNA-seq in tumor tissues of patients with luminal type breast cancer based on the TCGA database (N=998) according to Spearman's rank correlation. c Schematic diagram of the regulatory mechanisms of NSDHL knockdown in maintaining the BCSC population and tumor-initiating capacity in ER+ breast cancer

IV. Discussion

Accumulated reports have shown that cholesterol and rate-limiting enzymes of cholesterol biosynthesis are crucial for the maintenance and propagation of cancer stem cells in diverse cancers, including breast cancer [12-14, 16, 18, 26, 27]. We reported the NSDHL gene as a biomarker of poor prognosis to accelerate primary tumor growth and metastasis [21]. Therefore, with this special property, we hypothesized that NSDHL gene can be also involved in the maintenance and propagation of BCSCs. The siRNA/shRNA-mediated knockdown of the NSDHL gene inhibited spheroid formation of ER+ breast cancer cells grown on ultra-low attachment plates and tumorigenesis in an orthotopic breast cancer mouse model, and led to a reduction in BCSCs/progenitors with CD44+/ CD24- and EpCAM+/CD49f+ phenotypes and high ALDH activity in in vitro spheroids and in vivo xenograft tumors.

Depletion of HMGCR and FDPS genes and drugs (lovastatin, alendronate/zoledronate, and squalestatin 1) targeting specific HMGCR, FDPS, and FDFT1 enzymes impair spheroid formation in colon cancer and glioblastoma [15, 17], implying an important role of cholesterol biosynthesis genes in stemness and tumorigenesis. In present study, lovastatin, employed as an HMCGR inhibitor,

suppressed spheroid formation of MCF-7 (Fig. 4b). As we hypothesized, knockdown of the NSDHL gene led to the inhibition of tumor spheroid formation of MCF-7, ZR-75-1, and BT-474 grown on polymer-X-coated ultra-low attachment plates as well as a delay of tumor initiation in a mouse tumor model by injecting MCF-7 spheroids. We suggest that breast cancer cells rely on NSDHL to form BCSC-enriched spheroids and support their tumor initiation, thus promoting breast tumor development and progression.

The most commonly used markers of BCSCs are CD44+, CD24-/low, CD49f+, and EpCAM+ [1]. The majority of BCSCs with CD44+/CD24-/low phenotype exist mainly in luminal progenitors with the EpCAM+/CD49f+ phenotype [28]. Another BCSC is identified by its high ALDH activity [29]. We found that NSDHL knockdown reduced the BCSCs with CD24-/CD44+ phenotype and high ALDH activity and progenitors with the EpCAM+/CD49f+ phenotype in an ultra-low attachment in vitro culture system and xenograft tumors, thus substantiating NSDHL's critical role in BCSC maintenance.

Stemness, known as the self-renewal capacity of cancer stem cells, is regulated by many signaling pathways, including TGF-β, Hedgehog, Wnt, Notch, and FGF, and transcription factors including NANOG, OCT4, SOX2, KLF4, and c-MYC [30]. In the present

study on KEGG pathway analysis based on RNA-seq, the TGFβ signaling pathway was enriched in NSDHL-knockdown spheroids of MCF-7 cells, implying a link between the NSDHL and TGFβ signaling pathways in the regulation of BCSCs. We observed a decrease in the secretion of TGFβ 1 and TGFβ 3 in NSDHL-knockdown MCF-7 spheroids relative to the control, suggesting that NSDHL may be involved in TGFβ secretion. Further studies are required to explore the mechanism by which NSDHL regulates TGFβ, especially in terms of expression and secretion.

A decrease in TGFβ-mediated collagen fibrils and fibronectin production can inhibit spheroid-forming efficiency [31, 32]. Concurrently, we found a decrease in TGFβ 1 and TGFβ 3 with a simultaneous decrease in the mRNA expression of collagen I/IV and fibronectin splicing variant EDB-FN fibronectin, consequently impairing spheroid formation in NSDHL-knockdown MCF-7 spheroids relative to the control.

Recently, evidence for a connection between the genetic and pharmacological inhibition of cholesterol biosynthesis and TGFβ-mediated signaling pathways in the context of cancer stem cell maintenance and cancer progression to metastasis has emerged [15, 21, 33]. Treatment with atrovastatin or NSDHL knockout activates

SREBP1, which promotes TGFβ1 expression and induces a canonical Smad2 and Smad3 effector cascade, resulting in the induction of epithelial-mesenchymal transition in pancreatic cancer [12]. Contrary to the findings on NSDHL-knockdown pancreatic cancer cells, Chen M. et al. reported that NSDHL knockdown impairs the TGFβ-mediated Smad3 signaling pathway by inducing the endosomal degradation of TGFβ receptor 2 to serve as a promoter of cancer cell proliferation and metastasis in breast cancer cells (MDA-MB-231) [33]. In light of the aforementioned studies, the TGFβ-mediated molecular mechanisms by which NSDHL regulates the biological activities of cancer cells may differ between carcinomas.

The molecular mechanisms linking NSDHL and TGFβ-mediated signaling to the enrichment and maintenance of BCSCs remain poorly understood. Resultantly, we suggest that NSDHL is involved in the maintenance of BCSCs as well as cancer progression by activating TGFβ/Smad-mediated signaling in breast cancer. Mechanistically, NSDHL knockdown impaired tumor initiating and progression characteristics of BCSCs by suppressing TGFβ signaling, which in turn decreased the secretion of TGFβ 1 and TGFβ 3, inactivated Smad2 and Smad3, and downregulated the

expression of SOX2 and NANOG, key regulators of cancer stemness (Fig. 13c). We first observed that the stemness-related transcription factors, SOX2 and NANOG, in the context of TGFβ downstream signaling cascade, were significantly downregulated in NSDHL-knockdown breast cancer, a finding consistent with the TGFβ-mediated signaling to enrich and maintain the stemness of cancer cells and suggested that genetic and pharmacological targeting of NSDHL may be a potential therapy for eliminating BCSCs by inhibiting or abrogating their stemness.

Collectively, NSDHL is involved in TGFβ secretion, modulates TGFβ-mediated Smad signaling and expression of stemness-related genes SOX2, and NANOG, and is responsible for maintaining BCSCs with CD44+/CD24- phenotype and high ALDH activity and progenitors with EpCAM+/CD49f+ phenotype in in vitro tumor spheroids and in vivo xenograft tumor tissues. To our knowledge, our study is the first to show that NSDHL is responsible for maintaining the characteristics of BCSCs. However, cholesterol is an essential component in cell membrane and maintains cell homeostasis related with TGFβ signaling pathway. In our study we focused on ER+ breast cancer and has not been precisely elucidated between cholesterol and BCSCs relation to TGFβ signaling pathway. Further studies still need to be performed the

potential effect between cholesterol and BCSCs in breast cancer to deeply investigate the genetic networks and also finding to understand the roles of NSDHL in profoundly regulating BCSCs in breast tumor tissues of patients.

V. Conclusion

Collectively, NSDHL is involved in TGFβ secretion, modulates TGFβ-mediated Smad signaling and expression of stemness-related genes SOX2, and NANOG, and is responsible for maintaining BCSCs with CD44+/CD24- phenotype and high ALDH activity and progenitors with EpCAM+/CD49f+ phenotype in in vitro tumor spheroids and in vivo xenograft tumor tissues. To our knowledge, our study is the first to show that NSDHL is responsible for maintaining the characteristics of BCSCs. We suggest that genetic and pharmacological targeting of NSDHL may be a potential therapy for eliminating BCSCs by inhibiting or abrogating their stemness.

VI. References

1. Al-Hajj M, Wicha MS, Benito-Hernandez A, Morrison SJ, Clarke MF: Prospective identification of tumorigenic breast cancer cells. Proc Natl Acad Sci U S A 2003, 100(7):3983-3988.

2. Ginestier C, Hur MH, Charafe-Jauffret E, Monville F, Dutcher J, Brown M, Jacquemier J, Viens P, Kleer CG, Liu S et al: ALDH1 is a marker of normal and malignant human mammary stem cells and a predictor of poor clinical outcome. Cell Stem Cell 2007, 1(5):555-567.

3. Hu J, La Vecchia C, de Groh M, Negri E, Morrison H, Mery L, Canadian Cancer Registries Epidemiology Research G: Dietary cholesterol intake and cancer. Ann Oncol 2012, 23(2):491-500.

4. Yang L, Shi P, Zhao G, Xu J, Peng W, Zhang J, Zhang G, Wang X, Dong Z, Chen F et al: Targeting cancer stem cell pathways for cancer therapy. Signal Transduct Target Ther 2020, 5(1):8.

5. Kuzu OF, Noory MA, Robertson GP: The Role of Cholesterol in Cancer. Cancer Res 2016, 76(8):2063-2070.

6. Huang B, Song BL, Xu C: Cholesterol metabolism in cancer: mechanisms and therapeutic opportunities. Nat Metab 2020, 2(2):132-141.

7. Murai T, Maruyama Y, Mio K, Nishiyama H, Suga M, Sato C:

Low cholesterol triggers membrane microdomain-dependent CD44 shedding and suppresses tumor cell migration. J Biol Chem 2011, 286(3):1999-2007.

8. Babina IS, McSherry EA, Donatello S, Hill AD, Hopkins AM: A novel mechanism of regulating breast cancer cell migration via palmitoylation-dependent alterations in the lipid raft affiliation of CD44. Breast Cancer Res 2014, 16(1):R19.

9. Yang Z, Qin W, Chen Y, Yuan B, Song X, Wang B, Shen F, Fu J, Wang H: Cholesterol inhibits hepatocellular carcinoma invasion and metastasis by promoting CD44 localization in lipid rafts. Cancer Lett 2018, 429:66-77.

10. Chen CL, Huang SS, Huang JS: Cholesterol modulates cellular TGF-beta responsiveness by altering TGF-beta binding to TGF-beta receptors. J Cell Physiol 2008, 215(1):223-233.

11. Woosley AN, Dalton AC, Hussey GS, Howley BV, Mohanty BK, Grelet S, Dincman T, Bloos S, Olsen SK, Howe PH: TGFbeta promotes breast cancer stem cell self-renewal through an ILEI/LIFR signaling axis. Oncogene 2019, 38(20):3794-3811.

12. Gabitova-Cornell L, Surumbayeva A, Peri S, Franco-Barraza J, Restifo D, Weitz N, Ogier C, Goldman AR, Hartman TR, Francescone R et al: Cholesterol Pathway Inhibition Induces TGF-beta Signaling to Promote Basal Differentiation in Pancreatic Cancer.

Cancer Cell 2020, 38(4):567–583 e511.

13. Ginestier C, Monville F, Wicinski J, Cabaud O, Cervera N, Josselin E, Finetti P, Guille A, Larderet G, Viens P et al: Mevalonate metabolism regulates Basal breast cancer stem cells and is a potential therapeutic target. Stem Cells 2012, 30(7):1327–1337.

14. Ehmsen S, Pedersen MH, Wang G, Terp MG, Arslanagic A, Hood BL, Conrads TP, Leth–Larsen R, Ditzel HJ: Increased Cholesterol Biosynthesis Is a Key Characteristic of Breast Cancer Stem Cells Influencing Patient Outcome. Cell Rep 2019, 27(13):3927–3938 e3926.

15. Gao S, Soares F, Wang S, Wong CC, Chen H, Yang Z, Liu W, Go MYY, Ahmed M, Zeng Y et al: CRISPR screens identify cholesterol biosynthesis as a therapeutic target on stemness and drug resistance of colon cancer. Oncogene 2021, 40(48):6601–6613.

16. Wang B, Rong X, Palladino END, Wang J, Fogelman AM, Martin MG, Alrefai WA, Ford DA, Tontonoz P: Phospholipid Remodeling and Cholesterol Availability Regulate Intestinal Stemness and Tumorigenesis. Cell Stem Cell 2018, 22(2):206–220 e204.

17. Kim HY, Kim DK, Bae SH, Gwak H, Jeon JH, Kim JK, Lee BI, You HJ, Shin DH, Kim YH et al: Farnesyl diphosphate synthase is

important for the maintenance of glioblastoma stemness. Exp Mol Med 2018, 50(10):1-12.

18. Qiu T, Cao J, Chen W, Wang J, Wang Y, Zhao L, Liu M, He L, Wu G, Li H et al: 24-Dehydrocholesterol reductase promotes the growth of breast cancer stem-like cells through the Hedgehog pathway. Cancer Sci 2020, 111(10):3653-3664.

19. Tate R, Zona E, De Cicco R, Trotta V, Urciuoli M, Morelli A, Baiano S, Carnuccio R, Fuggetta MP, Morelli F: Simvastatin inhibits the expression of stemnessrelated genes and the metastatic invasion of human cancer cells via destruction of the cytoskeleton. Int J Oncol 2017, 51(6):1851-1859.

20. Lo CS, Sanii S, Kroeger DR, Milne K, Talhouk A, Chiu DS, Rahimi K, Shaw PA, Clarke BA, Nelson BH: Neoadjuvant Chemotherapy of Ovarian Cancer Results in Three Patterns of Tumor-Infiltrating Lymphocyte Response with Distinct Implications for Immunotherapy. Clin Cancer Res 2017, 23(4):925-934.

21. Yoon SH, Kim HS, Kim RN, Jung SY, Hong BS, Kang EJ, Lee HB, Moon HG, Noh DY, Han W: NAD(P)-dependent steroid dehydrogenase-like is involved in breast cancer cell growth and metastasis. BMC Cancer 2020, 20(1):375.

22. Nelson ER, Wardell SE, Jasper JS, Park S, Suchindran S, Howe MK, Carver NJ, Pillai RV, Sullivan PM, Sondhi V et al: 27-

Hydroxycholesterol links hypercholesterolemia and breast cancer pathophysiology. Science 2013, 342(6162):1094-1098.

23. Harborg S, Heide-Jorgensen U, Ahern TP, Ewertz M, Cronin-Fenton D, Borgquist S: Statin use and breast cancer recurrence in postmenopausal women treated with adjuvant aromatase inhibitors: a Danish population-based cohort study. Breast Cancer Res Treat 2020, 183(1):153-160.

24. Quinlan AR, Hall IM: BEDTools: a flexible suite of utilities for comparing genomic features. Bioinformatics 2010, 26(6):841-842.

25. Gentleman RC, Carey VJ, Bates DM, Bolstad B, Dettling M, Dudoit S, Ellis B, Gautier L, Ge Y, Gentry J et al: Bioconductor: open software development for computational biology and bioinformatics. Genome Biol 2004, 5(10):R80.

26. Jun SY, Brown AJ, Chua NK, Yoon JY, Lee JJ, Yang JO, Jang I, Jeon SJ, Choi TI, Kim CH et al: Reduction of Squalene Epoxidase by Cholesterol Accumulation Accelerates Colorectal Cancer Progression and Metastasis. Gastroenterology 2021, 160(4):1194-1207 e1128.

27. Wang X, Huang Z, Wu Q, Prager BC, Mack SC, Yang K, Kim LJY, Gimple RC, Shi Y, Lai S et al: MYC-Regulated Mevalonate Metabolism Maintains Brain Tumor-Initiating Cells. Cancer Res

2017, 77(18):4947-4960.

28. Ghebeh H, Sleiman GM, Manogaran PS, Al-Mazrou A, Barhoush E, Al-Mohanna FH, Tulbah A, Al-Faqeeh K, Adra CN: Profiling of normal and malignant breast tissue show CD44high/CD24low phenotype as a predominant stem/progenitor marker when used in combination with Ep-CAM/CD49f markers. BMC Cancer 2013, 13:289.

29. Marcato P, Dean CA, Pan D, Araslanova R, Gillis M, Joshi M, Helyer L, Pan L, Leidal A, Gujar S et al: Aldehyde dehydrogenase activity of breast cancer stem cells is primarily due to isoform ALDH1A3 and its expression is predictive of metastasis. Stem Cells 2011, 29(1):32-45.

30. Hadjimichael C, Chanoumidou K, Papadopoulou N, Arampatzi P, Papamatheakis J, Kretsovali A: Common stemness regulators of embryonic and cancer stem cells. World J Stem Cells 2015, 7(9):1150-1184.

31. Javelaud D, Alexaki VI, Dennler S, Mohammad KS, Guise TA, Mauviel A: TGF-beta/SMAD/GLI2 signaling axis in cancer progression and metastasis. Cancer Res 2011, 71(17):5606-5610.

32. Tian J, Hachim MY, Hachim IY, Dai M, Lo C, Raffa FA, Ali S, Lebrun JJ: Cyclooxygenase-2 regulates TGFbeta-induced cancer stemness in triple-negative breast cancer. Sci Rep 2017, 7:40258.

33. Chen M, Zhao Y, Yang X, Zhao Y, Liu Q, Liu Y, Hou Y, Sun H, Jin W: NSDHL promotes triple-negative breast cancer metastasis through the TGFbeta signaling pathway and cholesterol biosynthesis. Breast Cancer Res Treat 2021, 187(2):349-362.

국문 초록

NSDHL 유전자는 유방암세포에서 스페로이드 형성 및 종양 성장과 전이를 감소시키는 역할을 하지만 아직 줄기세포 기능 조절과 관련된 분자 기전에 대해서 연구된 바가 없기 때문에 본 연구에서는 호르몬 수용체 양성 유방암에서 NSDHL 유전자의 발현을 조절한 후 유방암 줄기세포에 미치는 영향과 이를 조절하는 기전에 대해 규명하였다. 호르몬 유방암 세포에서 NSDHL 유전자의 발현을 조절한 후 표면자극유도 플랫폼 기술을 적용한 특수 3D 스페로이드 플레이트에서 배양하여 스페로이드 형성 능력을 확인하였고. NSDHL이 억제 된 세포에서 스페로이드 형성 능력이 감소되는 것을 관찰하였다. NSDHL이 넉다운 된 MCF-7의 스페로이드와 대조군 스페로이드의 RNA sequencing 데이터에서 TGFβ와 관련된 617개의 유전자가 다르게 발현하는 것을 확인하였다. NSDHL-넉다운 스페로이드를 주입한 동소 종양 모델에서 대조군과 비교하여 종양 개시와 성장 능력이 매우 감소하였다. 유방암 줄기세포 모집단인 CD44+/CD24- 및 CD49f+/EpCAM+ 표현형과 높은 ALDH 활성도가 NSDHL-넉다운 스페로이드와 마우스모델 종양에서 감소되고, 이와 더불어 TGFβ 1과 3의 분비와 Smad2/3의 인산화 및 SOX2의 발현이 감소하였다. 또한, 유방암 환자의 표본에서 NSDHL과 SOX2의 양의 상관관계를 확인하였다. 본 연구의 결과는 NSDHL이 유방암 줄기세포 모집단 및 종양 개시 능력을 유지하는데 중요한 역할을 한다는 것을 밝혔으며,

NSDHL이 유방암 줄기세포를 억제하여 유방암의 개시 및 진행을 예방하는 표적 치료제임을 제시한다.

주요어 : 유방암, NSDHL, TGFβ, 암줄기세포, 콜레스테롤, 종양 스페로이드

학번 : 2020-36557